Chan–Vese Segmentation: A FIJI Plugin Implementation

Heitor Mynssen[1,2,3]

[1]Metabio, Instituto de Física, Universidade Federal do Rio de Janeiro, Brasil
[2]Rede Brasileira de Neurobiodivesidade, Instituto de Física, Universidade Federal do Rio de Janeiro, Brasil
[3]Instituto de Ciências Biomédicas, Universidade Federal do Rio de Janeiro, Brasil
Email: hmynssen@ufrj.br

Abstract

This report is the final exam for BMM771—Aquisição e processamento de imagem biológica. It details the implementation if a Fiji plugin for the Chan–Vese segmentation using two regions of interest. We will explore the Chan-Vese method, its theoretical foundation in image analysis and apply it to process brain MRI data of a human and a grey seal. This pdf and the source code is available at https://github.com/hmynssen/CV-Segmentation-FIJI.

Keywords

Segmentation, Chan–Vese, Fiji, BMM771

1 Introduction

Image segmentation is often a fundamental step in neuroanatomy and neuroimaging research. The classification of different tissue types enables analyses such as surface reconstruction (Fischl, 2012; Mynssen et al., 2024), which in turn supports further investigations of aging and disease (de Moraes et al., 2024), theoretical models of cortical folding (Wang et al., 2019, 2024), compared neuroanatomy (Mars et al., 2018; Boch et al., 2024), and others.

Among the various segmentation approaches, variational methods based on level-set formulations have gained prominence due to their mathematical foundation, relatively easy implementation, and absence of calibration or training. Within this family, the Chan–Vese (CV) active contour model (Chan and Vese, 2001) is one of the first and remains one of the most widely used because it does not rely on image gradients and performs well even when boundaries are poorly defined.

Given the necessity of image segmentation in so many different fields of research, this project presents an implementation of the two-level Chan–Vese model as a Fiji plugin for 2D 8-bit image segmentation. Also, the plugin was tested with two different subjects, one a human and another a grey seal, on their respective mid-coronal MRI slices.

Additionally, with the goal to provide a clear and reproducible reference for students, professors and researchers seeking to understand Chan–Vese and/or Fiji plugins, this report provides a theoretical background and the source code.

2 Theoretical Background

This section was divided into two main concepts to further improve the comprehension of the Chan–Vese algorithm implementation. Firstly, we revisit classical physics and variational calculus to, secondly, dive into the application of those concepts for the Chan–Vese image segmentation.

2.1 Functional Formulation and Euler–Lagrange Solution

Developing a mathematical formulation to describe the underlying mechanics of a system is a crucial step in any area of physics. It can be said that the first such formulation was given to us in the form laws of motion and gravitation by Newton, in his most famous work *Principia Mathematica*. In sense, those set of equations, like "$\mathbf{F} = m\mathbf{a}$", is sufficient to solve any system given enough patience and/or computational power. However, being sufficient in theory is far from ideal, and, additionally, it also hides certain features of the natural systems being studied.

To solve those issues, Euler, Hamilton, Lagrange and many others have come up with alternatives to derive the mechanics of various systems. Eventually, after over a century of scientific development, we arrive at the **principle of least action**, which will form the basis of many modern physics sub-fields.

This section will use the standard exposition found in analytical mechanics Lemos (2000); Taylor (2005); Feynman et al. (1964).

From Classical Mechanics to Calculus of Variations

A major realization, over the Newtonian mechanics, was that many physical systems can be described globally, not locally, through the extremization of a single scalar quantity: the action. In this perspective, a system moving between two configurations, like a particle from initial to final position, could explore an infinite set of possible trajectories. The *physical* trajectory is then se-

lected by requiring that the action functional

$$S[q] = \int_{t_0}^{t_1} L(q, \dot{q}, t)\, dt \tag{1}$$

is stationary with respect to variations of $q(t)$. This principle represents a profound shift: the laws of dynamics emerge from a single scalar quantity rather than from a vector equation.

In practice, to find such trajectory we have to utilize variational calculus. In our case for the action, we consider the following:

- fixed initial and final positions;
- perturbations in the position of the form $q(t) \to q(t) + \delta q(t)$;
- and, finally, that $\delta S = 0$, i.e. the action is an extremum.

Applying the above conditions to equation 1, we arrive at the famous Euler-Lagrange equation:

$$\frac{d}{dt}\left(\frac{\partial L}{\partial \dot{q}}\right) - \frac{\partial L}{\partial q} = 0. \tag{2}$$

This new equation[2] expresses a universal rule: among all possible trajectories connecting two configurations, the physical one is the curve that makes the action stationary. Although rooted in mechanics, this idea extends far beyond the motion of particles. Any system that can be described by an energy or cost functional (from elastic membranes to biochemical reaction pathways) can be studied through the same variational principle. The details of the physics may vary, but the mathematics remains identical: find the configuration that minimizes (or extremizes) a functional.

This viewpoint is particularly helpful for researchers outside physics because it shifts attention away from forces and toward *optimization*. Instead of asking "What pushes the system?", we ask "What configuration minimizes the relevant quantity?" In classical mechanics this quantity is the action; in structural biology it may be protein folding energy; in neuroscience it may be a wiring or metabolic cost; and in image analysis it becomes a measure of contour length and regional homogeneity. The unifying theme is that systems tend to evolve toward states that optimize an energy-like functional.

In this sense, active contour models (including the Chan–Vese method) can be understood as biological cousins of variational mechanics. A contour evolves not because of a physical force, but because the algorithm continuously adjusts it to decrease a well-defined functional measuring how well the curve separates regions of interest. The mathematics behind its evolution is precisely the Euler–Lagrange equation applied to an image-based functional. Thus, even though the context here is neuroanatomy rather than classical physics, the conceptual bridge is the same: a system follows the path of least "action", or, in this case, least segmentation energy.

Chan-Vese Functional Formulation

Having introduced the variational viewpoint from classical mechanics, we now carry the same logic over to image segmentation. Instead of a particle trajectory, we study a contour that moves across an image. Instead of an action, we define an energy functional whose minimum corresponds to the "best" segmentation according to the model.

To understand how this is done, we consider an image $I(x, y)$, where x, y correspond to the coordinates of the pixels in the image, and a sub-region $\phi(x, y)$ contained in the image that delimits the frontier between the inside and outside of the segmentation. Using these two mathematical objects, the Chan–Vese model (Chan and Vese, 2001) defines the functional to be minimized, and therefore determines the evolution of the contour, as:

$$\begin{aligned} E(\phi, c_1, c_2) = \mu \int_\Omega |\nabla H(\phi)|\, dx + \\ \nu \int_\Omega H(\phi)\, dx + \\ \lambda_1 \int_\Omega (I - c_1)^2 H(\phi)\, dx + \\ \lambda_2 \int_\Omega (I - c_2)^2 (1 - H(\phi))\, dx, \end{aligned}$$

where H is the Heaviside function of ϕ, and c_1 and c_2 represent the mean brightness intensities inside and outside the contour, respectively. The first term penalizes long or irregular boundaries, and it is controlled by the parameter μ. The second term is the inflation term, that regularizes the growth of the segmentation area, and is controlled by ν. The third and forth terms penalize poor intensity fitting inside and outside the region, and are controlled by the parameters λ_1 and λ_2 respectively.

Minimizing this functional follows the same recipe outlined in the previous section. In this case, the resulting gradient-flow evolution equation becomes

$$\frac{\partial \phi}{\partial t} = \delta(\phi)\Big[\mu\, \kappa(\phi) - \lambda_1 (I - c_1)^2 + \lambda_2 (I - c_2)^2 + \nu\Big], \tag{3}$$

where δ is a smooth approximation of the Dirac delta, and $\kappa(\phi)$ is the curvature of the level set. Just as in classical mechanics the system moves toward the path that makes the action stationary, here the contour moves in the direction that decreases this segmentation energy.

This formulation turns the evolution of a digital contour into a problem formally similar to the motion of a physical system under a variational principle. For biological imaging, this perspective is extremely useful: it provides a principled and transparent way to incorporate desired properties (such as smoothness, region consistency, or robustness to noise) directly into the functional. Once the functional is defined, the segmentation contour emerges naturally from its minimization, much like the physical trajectory emerges from the principle of least action.

2.2 The Chan-Vese Algorithm

The continuous partial differential equation (3) is solved iteratively using a time-marching numerical scheme.

This process alternates between calculating the optimal region means (c_1, c_2) and updating the level-set function (ϕ).

This iterative process continues until the change in ϕ falls below a predefined tolerance or a maximum number of iterations is reached. The final zero-level set C represents the segmented boundary.

3 Material and Methods

3.1 Image Data

Two sets of brain MRI data were used to test the segmentation pipeline, focusing on the mid-coronal slice of each image (2D 8-bit).

- **Human Subject:** Data extracted from a single subject (subj-0000) from the AHEAD (Amsterdam Ultra-high field adult lifespan database) dataset (Alkemade et al., 2020). The brain extraction and initial structural processing were performed using FreeSurfer (Fischl, 2012).
- **Grey Seal *(Halichoerus grypus)*:** Data derived from a high-resolution grey seal brain (Hoeksema et al., 2021), representing a distinct comparative neuroanatomy challenge.

The choice of subjects provides two structurally distinct brains, allowing the evaluation of the Chan-Vese method's robustness to varying gray matter, white matter, and CSF contrast levels. In both cases, the midmost coronal slice was selected visually and was set as the 2D image to segment.

3.2 Implementation Details

The Chan-Vese segmentation algorithm was implemented as an ImageJ/Fiji plugin using Java, and is available at https://github.com/hmynssen/CV-Segmentation-FIJI. The implementation adheres to the numerical scheme derived from the minimization of the energy functional.

1. Pre-processing and Initialization

- **Image Normalization:** The input image (8, 16, or 32-bit) is converted to a `FloatProcessor` and normalized by its maximum intensity, ensuring pixel values $I \in [0, 1]$.
- **Initial Level Set (ϕ):** The level set function ϕ is initialized as a signed distance function (SDF).
  - If an ImageJ ROI exists, ϕ is set to a negative constant (inside ROI) and a positive constant (outside ROI).
  - Otherwise, a central circle with a radius equal to 50% of the minimum image dimension is used as the initial contour, setting ϕ according to the distance from this circle.

2. Iterative Evolution The `chanVeseIteration` loop executes for `MAX_ITERATIONS` steps, updating ϕ at each time step Δt (`TIME_STEP`).

1. **Mean Intensity Calculation (c_1, c_2):** The region means are calculated based on the current partitioning: c_1 (inside, $\phi < 0$) and c_2 (outside, $\phi \geq 0$).

$$c_1 = \text{mean}(I \mid \phi^t < 0), \qquad c_2 = \text{mean}(I \mid \phi^t > 0).$$

2. **Curvature Calculation (κ):** The curvature at each pixel (x, y) is computed using a centered finite difference approximation on ϕ with periodic boundary conditions. The formula used is:

$$\kappa(\phi) = \frac{\phi_{xx}\phi_y^2 - 2\phi_x\phi_y\phi_{xy} + \phi_{yy}\phi_x^2}{|\nabla\phi|^2}$$

where the denominators are regularized to avoid division by zero.

3. **Brightness Data-fitting:** The data-fitting terms are determined by the squared intensity differences: $F_1 = (I - c_1)^2$ and $F_2 = (I - c_2)^2$.

4. **Level Set Update:** The level set is updated using the explicit Euler scheme:

$$\phi^{t+1} = \phi^t + \Delta t\ \delta(\phi)[\mu\kappa(\phi) + \lambda_1 F_1 - \lambda_2 F_2 + \nu]$$

with the following approximation for the Dirac-delta:

$$\delta(\phi_0) = \frac{\epsilon}{\pi(\epsilon^2 + \phi_0^2)}$$

4 Results

The Chan-Vese segmentation model was applied to the mid-coronal slices of a Human and a Grey Seal brain MRI, using the implemented Fiji plugin. The segmentation was initiated from a central circular Region of Interest (ROI) and ran for 5000 iterations with parameters $\epsilon = 1.0$, $\mu = 0.002$, $\lambda_1 = 25.0$, $\lambda_2 = 5.0$, and $\Delta t = 0.2$ for both subjects. Due to the difference in sizes of the brain, the Human subject had $\nu = 0.0$, while the Grey Seal had $\nu = 0.1$.

The results, presented in Figure 1, demonstrate the model's ability to delineate different tissues from the background. For both subjects, the curve successfully converged to the boundary, confirming the stability of the numerical scheme.

5 Discussion

The visual results presented in this work demonstrate the potential of the proposed region-based active contour model in accurately segmenting targets, even within images exhibiting significant background clutter or subtle boundary definitions. Our chosen approach leverages the strength of level-set evolution, providing a robust and topology-independent favoring balance between computational efficiency and segmentation fidelity.

Figure 1: Chan-Vese Segmentation Results for Human (upper row) and Grey Seal (lower row) Brain MRI. The columns represent the original grayscale image (left), segmented/masked image ($\phi < 0$ in teal; center), and final binary mask (right).

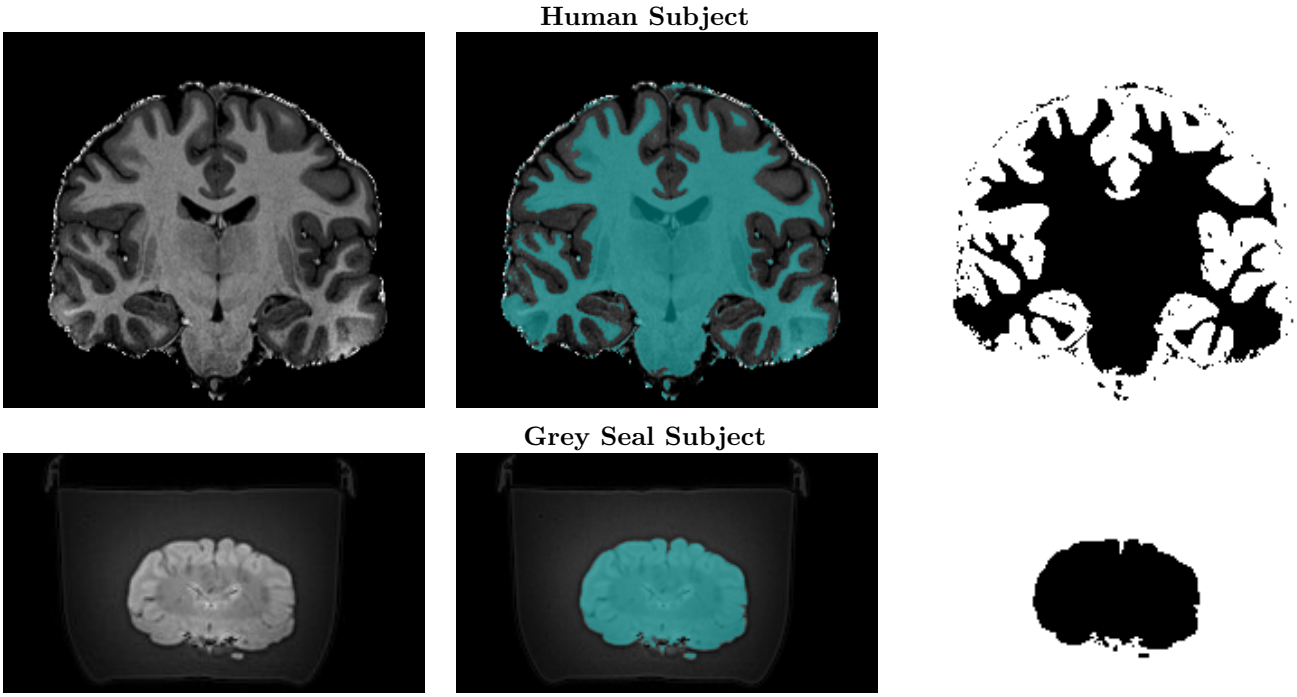

However, some difficulties and limitations must be addressed. From the results, it is possible to observe that different tissue types were segmented for basically the same choice of parameters. In the Human case, the setting provided a separation between white-matter and gray-matter. In the Grey Seal, however, the segmentation was focused on separating the whole brain from its surrounding medium. Another aspect of the model is that it remains inherently tied to the chosen kernel size and the initialization of the level-set function. This indicates that the tool requires considerable manual intervention from specialists to properly acquire the desired results by setting adequate initial conditions and parameters.

Lastly, regions with pronounced, non-smooth intensity variations may still pose yet another challenge, leading to convergence near local minima rather than the globally optimal boundary, despite careful parameter selection. This necessitates further exploration into regularization techniques that can maintain curve smoothness while strictly adhering to local data fitting, a common trade-off in variational approaches.

6 Conclusion

This work shows a solid framework for image segmentation using implicit active contours, even in images with non-uniform illumination. Subsequent extensions of the Chan-Vese (CV) model motivate future research: (1) Making the algorithm fully 3D for volumetric data processing, critical for MRI images; and (2) Implementing LBF (Li et al., 2007) and/or LGIF (Wang et al., 2009) models as auxiliary plugins to robustly account for local inhomogeneities in clinical datasets.

References

Alkemade, A., Mulder, M. J., Groot, J. M., Isaacs, B. R., van Berendonk, N., Lute, N., Isherwood, S. J., Bazin, P.-L., and Forstmann, B. U. (2020). The amsterdam ultra-high field adult lifespan database (ahead): A freely available multimodal 7 tesla submillimeter mri database. *NeuroImage*, 221:117200.

Boch, M., Karadachka, K., Loh, K. K., Benn, R. A., Roumazeilles, L., Bertelsen, M. F., Manger, P. R., Wrigglesworth, E., Spiro, S., Spocter, M. A., Johnson, P. J., Avelino-de Souza, K., Patzke, N., Lamm, C., Miller, K. L., Sallet, J., Khrapitchev, A. A., Tendler, B. C., and Mars, R. B. (2024). Comparative neuroimaging of the carnivoran brain: Neocortical sulcal anatomy. *eLife*, 13:RP100851.

Chan, T. F. and Vese, L. A. (2001). Active contours without edges. *IEEE Transactions on Image Processing*, 10(2):266–277.

de Moraes, F. H. P., Sudo, F., Monteiro, M. C., de Melo, B. R. P., Mattos, P., Mota, B., and Tovar-Moll, F. (2024). Cortical folding correlates to aging and alzheimer's disease's cognitive and csf biomarkers. *Scientific Reports*, 14(3222).

Feynman, R. P., Leighton, R. B., and Sands, M. (1964). *The Feynman Lectures on Physics, Vol. II.* Addison-Wesley.

Fischl, B. (2012). Freesurfer. *NeuroImage*, 62(2):774–781.

Hoeksema, N. et al. (2021). Neuroanatomy of the grey seal brain: bringing pinnipeds into the neurobiological study of vocal learning. *Philosophical Transactions of the Royal Society B: Biological Sciences*, 376(1836).

Lemos, N. A. (2000). *Mecânica Analítica*. UFF.

Li, C., Kao, C.-Y., Gore, J. C., and Ding, Z. (2007). Implicit active contours driven by local binary fitting energy. In *2007 IEEE Conference on Computer Vision and Pattern Recognition*, pages 1–7, Minneapolis, MN, USA.

Mars, R. B., Sotiropoulos, S. N., Passingham, R. E., Sallet, J., Verhagen, L., Khrapitchev, A. A., Sibson, N., and Jbabdi, S. (2018). Whole brain comparative anatomy using connectivity blueprints. *eLife*, 7:e35237.

Mynssen, H., Avelino-de Souza, K., Chaim, K., Ribeiro, V. L., Patzke, N., and Mota, B. (2024). Stitcher: A surface reconstruction tool for highly gyrified brains. *Neuroinformatics*, 22(4):539–554.

Taylor, J. (2005). *Classical Mechanics*. G - Reference,Information and Interdisciplinary Subjects Series. University Science Books.

Wang, L., Li, C., Sun, Q., Xia, D., and Kao, C.-Y. (2009). Active contours driven by local and global intensity fitting energy with application to brain mr image segmentation. *Computerized Medical Imaging and Graphics*, 33(7):520–531.

Wang, Y., Leiberg, K., Kindred, N., Madan, C. R., Poirier, C., Petkov, C. I., Taylor, P. N., and Mota, B. (2024). Neuro-evolutionary evidence for a universal fractal primate brain shape. *eLife*, 12:RP92080.

Wang, Y., Necus, J., Peraza Rodriguez, L., Taylor, P. N., and Mota, B. (2019). Human cortical folding across regions within individual brains follows universal scaling law. *Communications Biology*, 2:191.